# First-principles study of the Structural, Mechanical, Dynamical, Electronic and Lattice Thermal Conductivity properties of HfSnPt: A half-Heusler alloy

**Ibrahim O A Ali[1], B O Mnisi[1], E M Benecha[2] and M M Tibane[1]**

[1] Department of Physics, University of South Africa, Johannesburg, South Africa, 1709.
[2] College of Science, Engineering and Technology, University of South Africa, Johannesburg, South Africa, 1709.

E-mail: ibraphysics@gmail.com

**Abstract.** The density functional theory (DFT) is applied to systematically investigate the structural, electronic, mechanical, and vibrational properties of half-Heusler HfSnPt in its cubic phase. In this study, the phase stability of the HfSnPt alloy is investigated using formation energy, as well as its mechanical and vibrational properties. HfSnPt compound shows a negative heat of formation, indicating thermodynamic stability, which is consistent with it's cohesive energy. The mechanical properties are examined based on various characterization descriptors, including the independent elastic coefficients, bulk, shear, and Young's modulus, ratios such as Pugh and Poisson's, Kleinnman parameter, Zener anisotropy factor, and melting temperature. The equilibrium elastic constants satisfy all the mechanical stability criteria for cubic crystals. The analysis of band structures, reveals that HfSnPt alloy is a semiconductor with indirect band gap of 0.889 eV. Finally, the phonon calculations confirm that HfSnPt is dynamically stable. This compound exhibits thermodynamic, mechanical, and dynamic stability, along with a high melting point, making it a strong candidate for high-temperature structural applications.

## 1 Introduction

Thermoelectric (TE) materials can convert waste heat into electrical energy, offering a compact and reliable means of solid state power generation suitable for applications in microelectronics, automotive, and industrial systems [1]. The efficiency of a TE material is measured by the dimensionless figure of merit, $ZT = \alpha^2\sigma T/k$, where $\alpha$ is the Seebeck coefficient, $\sigma$ is the electrical conductivity, T is the absolute temperature, and $k$ is the thermal conductivity [2]. Materials with a figure of merit ($ZT$) close to 1 are considered promising; however, many of these compounds face challenges such as high-temperature instability, difficulties in synthesis, or toxicity concerns.however, many of these compounds face challenges such as high-temperature instability, difficulties in synthesis, or toxicity concerns. [3].

Among the various candidates, Half-Heusler (HH) alloys composed of cost-effective, lightweight, and environmentally friendly elements exhibit high power factors but are typically limited by their high lattice thermal conductivity [3, 4, 5]. HH compounds adopt the MgAgAs-type structure (space group F-43m) with a partially filled face-centered cubic (fcc) lattice [6], and their semiconducting behavior depends on the valence electron count [7].

Previous study has investigated the HfPtSn alloy, revealing its thermodynamic stability and semi-conducting nature [8]; however, detailed information on its mechanical and vibrational properties, as well as lattice thermal conductivity, remains underreported.The insights gained will clarify its suitability for thermoelectric and structural applications under extreme conditions [9].

## 2 Computational details

All calculations for the HfSnPt compound were performed using the Vienna Ab initio Simulation Package (VASP) within the framework of density functional theory (DFT). The generalized gradient approximation (GGA) with the Perdew–Burke–Ernzerhof (PBE) functional [10] was used to treat exchange-correlation effects. The projector augmented wave (PAW) method [11] was employed to describe the interactions between valence electrons and ionic cores.

To obtain a more accurate description of the electronic structure, especially near the Fermi level, the Heyd-Scuseria-Ernzerhof (HSE06) hybrid functional [12] was applied. This functional incorporates a portion of exact exchange and uses a screening parameter ($\mu$) of 0.1 $Å^{-1}$. Furthermore, spin–orbit coupling (SOC) effects were included due to the presence of heavy atoms like Hf and Pt, which introduce significant relativistic interactions. a $10\times10\times10$ kpoint meshes was used in sampling the Brillouin zone (BZ), with an energy cut-off of 600 eV, which was found to be sufficient for energy convergence. The convergence threshold for self-consistent field iteration was set at $10^{-8}$ eV.

The structural, mechanical, and electronic properties were derived from fully relaxed unit cells of HfSnPt. Phonon and thermodynamic properties were calculated using the finite displacement method implemented in the PHONOPY package [13], with a $2\times2\times2$ supercell and a $4\times4\times4$ Monkhorst-Pack k-point grid. The third-order force constants were computed via PHONO3PY [14], considering all symmetry-inequivalent atomic displacements (255 in total) without imposing cutoff limits. A $24\times24\times24$ q-point mesh was adopted to evaluate the lattice thermal conductivity accurately.

## 3 Results and discussion

### *3.1 Structural Properties*

The HfSnPt compound adopts the face-centered cubic $C1_b$ structure, belonging to the F43m space group. In this configuration, Hf atoms occupy the 4a Wyckoff position (0, 0, 0), Sn atoms are located at 4b (0.5, 0.5, 0.5), and Pt atoms reside at 4c (0.25, 0.25, 0.25). The atomic arrangement within the unit cell is depicted in Figure 1. The experimental lattice constant for HfSnPt is reported as 6.31 Å [15]. To determine its equilibrium geometry, the total energy was minimized with respect to volume using the PBE exchange-correlation functional. The optimization, performed at the ground state, yielded a lattice constant in close agreement with the experimental value.

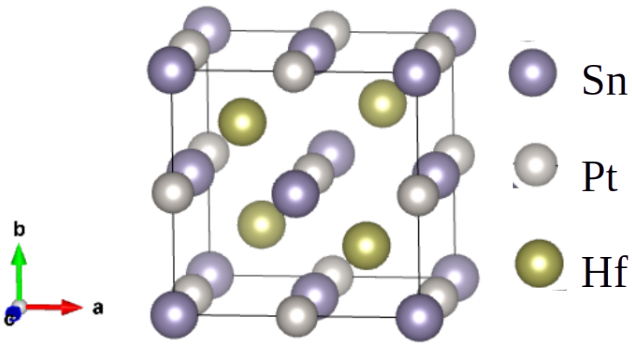


Figure 1: The crystal structure of HfSnPt half-Heusler compound

| X | Method | $a$ (Å) | $\rho$ (g/cm$^3$) | $\Delta H$ (eV/atom) | $E_{coh}$ (eV/atom) | $V_0$ (Å$^3$) | $B$ (GPa) | $B_0^{'}$ |
|---|---|---|---|---|---|---|---|---|
| HfSnPt | VASP | 6.38 | 12.59 | -0.45 | -5.99 | 259.69 | 139.25 | 4.65 |
| HfSnPt | Exp. [15] | 6.31 | ... | .... | .... | .... | .... | |

Table 1: The lattice parameter ($a$), density ($\rho$), formation energy ($\Delta$ H), cohesive energy ($E_{coh}$), equilibrium volume V (Å$^3$), bulk modulus (B), and Bulk derivatives ($B_0^{'}$) of the investigated cubic HfSnPt in this study are compared with available experimental values.

The calculated structural properties for HfSnPt are summarized in Table 1, including lattice constant, density, formation energy, cohesive energy, and bulk modulus. We note that the formation energy of HfSnPt alloy is negative (-0.45 eV), indicating thermodynamic stability. Additionally, its cohesive energy is -5.99 eV/atom, suggesting good structural integrity.

The density of HfSnPt is predicted to be approximately 12.59 g/cm$^3$, which is relatively high compared to several engineering materials. For instance, it surpasses that of $Ni_3Al$ (6.14 g/cm$^3$) [16], a known lightweight alloy, and is comparable to dense materials such as $HfB_2$ (11.20 g/cm$^3$) [17]. This high density might limit its applicability in weight-sensitive applications despite its promising stability.

### *3.2 Electronic Properties*

The electronic band structure and density of states (DOS) calculations reveal that HfSnPt is a semiconductor with an indirect band gap. The valence band maximum (VBM) occurs at the Γ-point, while the conduction band minimum (CBM) is located at the X-point as shown in Figure 2, confirming its indirect band gap nature. Using the GGA functional, the band gap is approximately 0.889 eV, which narrows to 0.664 eV when spin-orbit coupling (SOC) is included. In contrast, the HSE06 hybrid functional predicts a wider gap of about 1.22 eV as shown in Table 2, consistent with the known tendency of GGA to underestimate band gaps [18]. Despite all constituent

| X | Method | GGA | GGA+SOC | HSE06 |
|---|---|---|---|---|
| HfSnPt | VASP | 0.889 | 0.664 | 1.22 |

Table 2: Comparison of calculated energy band gaps (in eV) for HfSnPt using various first-principles codes and functionals.

elements being metallic in their elemental form. The observed semiconducting behavior is attributed to the 18-electron rule and the ordered cubic $C1_b$ structure, which promote a filled valence band and an empty conduction band. While indirect semiconductors like HfSnPt have lower optical absorption than direct-gap materials, they offer longer carrier lifetimes and better thermal stability, making them promising candidates for thermoelectric devices, power electronics, and LEDs.

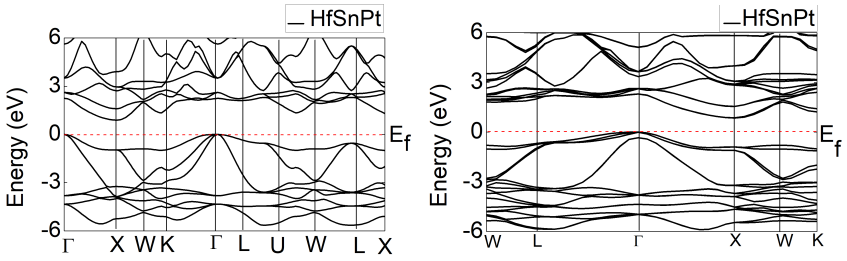


Figure 2: Calculated band structure of the HfSnPt alloy (*left*) using the GGA functional with the VASP code, and band structure (*right*) using GGA+SOC with the CASTEP code.

### *3.3 Mechanical Properties*

The mechanical properties of HfSnPt were assessed using elastic constants derived from first-principles calculations. The elastic constants values ( $C_{11}$, $C_{12}$, and $C_{44}$) for HfSnPt shown in Table 3, satisfy the Born criteria [19] as shown in equation 1, confirming the mechanical stability of the cubic phase. Its elastic constants are comparable to those of other robust intermetallics like TiNiSn and ZrNiSn [20].

$$C_{11} - C_{12} > 0; C_{11} + 2C_{12} > 0; C_{44} > 0. \tag{1}$$

Using the Voigt-Reuss-Hill approximation, the bulk modulus ($B$), shear modulus ($G$), and Young's modulus ($E$) for HfSnPt in Table 4 indicate high rigidity and low compressibility. These values are consistent with trends observed in solid solutions like $(Ti_{1-x}M_x)_2AlC$ [21], where heavier atoms increase bond strength and stiffness.

| X | Method | $C_{11}$ | $C_{12}$ | $C_{44}$ | $C_{12}$-$C_{44}$ | $\zeta$ | $T_m$(K) |
|---|---|---|---|---|---|---|---|
| HfSnPt | VASP | 214.99 | 104.05 | 75.18 | 28.85 | 0.81 | 1918 |

Table 3: Mechanical parameters of cubic HfSnPt whereby $C_{ij}$, $\zeta$, and $T_m(K)$ are the independent elastic coefficients in GPa, Kleinman parameter, and melting temperature.

| X | Method | $B_H$ | $G_H$ | $E_H$ | $E_H/G_H$ | $\nu$ | $A_\mu$ | $H_V$ |
|---|---|---|---|---|---|---|---|---|
| HfSnPt | VASP | 141.03 | 66.57 | 172.55 | 2.11 | 0.29 | 1.36 | 6.73 (7.04) |

Table 4: The calculated bulk moduli ( $B_H$ in GPa), shear moduli ( $G_H$ in GPa), Young's modulus ($E_H$ in GPa), $B_H/G_H$, Poisson's ratio $\nu$, Zener anisotropy factor $A_\mu$, and Vickers hardness ($H_V$ Chen (Tian) in GPa) of HfSnPt.

The Pugh's ratio (B/G) exceeds the critical value of 1.75, and Poisson's ratio is above 0.26, indicating a ductile behavior in HfSnPt alloy.. Additionally, the Cauchy pressure is positive, indicating metallic bonding and supporting the material's ductile behavior similar to trends in other ternary borides like $M_2GaB$ (M = Sc, V, Nb, Ta) [22]. The Kleinman parameter ($\zeta$) for HfSnPt is calculated to be 0.81, suggesting that bond-stretching dominates its deformation mechanism, consistent with behavior seen in high-valent borides [23]. Hardness estimates using both the Chen-Niu [24] and Tian [25] models place HfSnPt in the moderately hard category, with Vickers hardness values between 6.73 and 7.04 GPa depending on the model used. These results are consistent with comparable intermetallics such as ZnN and NiN [26]. The melting temperature, derived from the magnitude of $C_{11}$ as shown in equation 2 [27], is predicted to be higher than that of $Ni_3Al$ (1691 K) [16], implying strong thermal resistance and stability suitable for extreme environments, including turbine engines.

$$Tm = [553K + (5.9\text{K/GPa})C_{11}] + 300\text{K}. \tag{2}$$

Finally, the Zener anisotropy factor ($A_\mu$) of approximately 1.36 indicates slight elastic anisotropy significantly lower than layered materials like MAX phases [28], pointing to a more uniform mechanical response, which is favorable for structural applications.

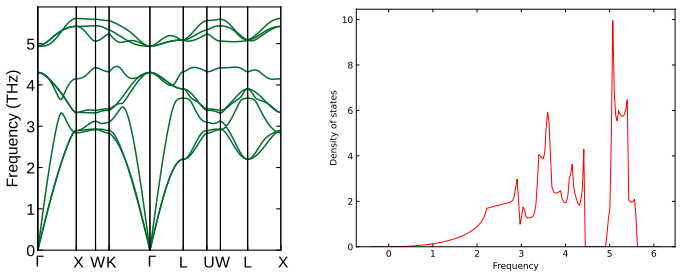


Figure 3: (*left*) Phonon dispersion curves of the HfSnPt. (*right*) phonon total density of states of the HfSnPt.

### *3.4 Phonon Properties*

Phonon calculations were carried out for HfSnPt using the finite displacement method [29], which is essential for evaluating its vibrational and thermodynamic behavior. The resulting phonon dispersion curves (PDC) and phonon density of states (PDOS) offer insight into the dynamic stability and thermal characteristics of the compound [13]. As shown in Figure 3, the phonon spectrum of HfSnPt displays no imaginary frequencies along high-symmetry paths of the Brillouin zone, confirming its dynamical stability at 0 K [13]. The absence of soft modes suggests that the structure is resistant to spontaneous lattice distortions or phase transitions. Moreover, the lowest vibrational modes originate from the acoustic branches near the $\Gamma$-point, a typical signature of dynamically stable intermetallics. The stable phonon profile supports the compound's predicted mechanical robustness and thermal reliability, indicating its potential for high-temperature structural applications.

### *3.5 Lattice thermal conductivity*

The lattice thermal conductivity ($k_l$) plays a vital role in determining a material's performance in both heat management and thermoelectric applications [30]. For HfSnPt, our first-principles calculations reveal a room-temperature value of approximately 16.4 W/m·K as shown in Figure 4, which is higher than that of traditional half-Heusler thermoelectrics like HfNiSn (14.6 W/m·K) [31]. This suggests that the presence of Pt strengthens the lattice, enhancing phonon transport. As temperature increases, $k_l$ for HfSnPt decreases due to phonon-phonon Umklapp scattering, dropping to about 4.9 W/m·K at 1000 K. The close values of $k_l$ along the $x-$, $y-$, and $z$-directions confirm isotropic thermal transport, consistent with the symmetry of the cubic structure. These findings indicate that HfSnPt, with its high thermal conductivity and isotropic behavior, could be well-suited for thermal dissipation

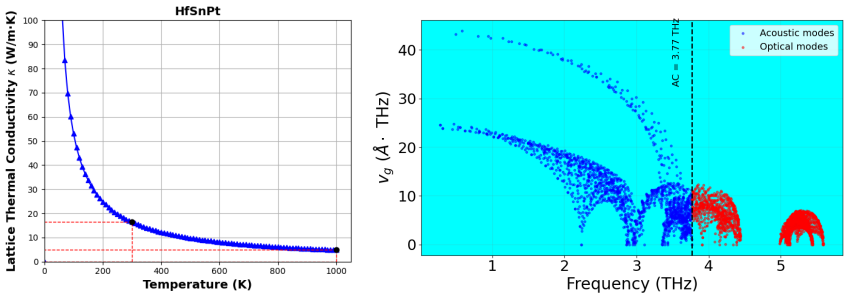


Figure 4: Calculated lattice thermal conductivity (*left*) and phonon group velocity (*right*) of HfSnPt.

in high-power or microelectronic devices, although its high $k_l$ may limit its effectiveness in thermoelectric energy conversion.

## 4 Conclusion

In this study, the structural, electronic, mechanical, phonon, and thermal properties of HfSnPt were investigated using first-principles calculations within the GGA framework implemented in the VASP code. The negative formation and cohesive energies confirm that HfSnPt is thermodynamically and structurally stable, indicating feasibility for experimental synthesis. Electronic band structure analysis revealed that HfSnPt is an indirect semiconductor. The SOC effect was found to slightly reduce the band gap, while calculations using the HSE06 hybrid functional predicted a broader gap, aligning with previous findings that hybrid functionals offer improved accuracy. Phonon dispersion results showed no imaginary frequencies, confirming the dynamical stability of HfSnPt. The compound also demonstrated mechanical stability and ductility, supported by a B/G ratio greater than 1.75 and a melting point exceeding 1900 K. At room temperature, the lattice thermal conductivity was calculated to be 16.4 W/m·K, decreasing with temperature due to enhanced Umklapp scattering, reaching approximately 4.9 W/m·K at 1000 K. This thermal behavior, along with its structural resilience, positions HfSnPt as a promising candidate for high-temperature structural and thermoelectric applications, particularly in environments requiring thermal stability and long service life, such as aerospace systems.

## References


[1] G. J. Snyder and E. S. Toberer, "Complex thermoelectric materials," *Nature materials*, vol. 7, no. 2, pp. 105–114, 2008.

[2] A. A. Khan, I. Khan, I. Ahmad, and Z. Ali, "Thermoelectric studies of IV–VI semiconductors for renewable energy resources," *Materials Science in Semiconductor Processing*, vol. 48, pp. 85–94, 2016.

[3] Q. Ren, C. Fu, Q. Qiu, S. Dai, Z. Liu, T. Masuda, S. Asai, M. Hagihala, S. Lee, S. Torri *et al.*, "Establishing the carrier scattering phase diagram for ZrNiSn-based half-Heusler thermoelectric materials," *Nature communications*, vol. 11, no. 1, p. 3142, 2020.

[4] S. Sakurada and N. Shutoh, "Effect of Ti substitution on the thermoelectric properties of (Zr, Hf) NiSn half-Heusler compounds," *Applied Physics Letters*, vol. 86, no. 8, 2005.

[5] F. Aliev, V. Kozyrkov, V. Moshchalkov, R. Scolozdra, and K. Durczewski, "Narrow band in the intermetallic compounds MNiSn (M= Ti, Zr, Hf)," *Zeitschrift für Physik B Condensed Matter*, vol. 80, pp. 353–357, 1990.

[6] W. Jeitschko, "Transition metal stannides with MgAgAs and $MnCu_2Al$ type structure," *Metallurgical Transactions*, vol. 1, pp. 3159–3162, 1970.

[7] Y. Kimura and Y.-W. Chai, "Ordered structures and thermoelectric properties of MNiSn (M= Ti, Zr, Hf)-based half-Heusler compounds affected by close relationship with heusler compounds," *Jom*, vol. 67, pp. 233–245, 2015.

[8] Y. G. Yu, X. Zhang, and A. Zunger, "Natural off-stoichiometry causes carrier doping in half-Heusler filled tetrahedral structures," *Physical Review B*, vol. 95, no. 8, p. 085201, 2017.

[9] H. Joshi, D. Rai, A. Laref, and R. Thapa, "Electronic, and thermoelectric properties of half-Heusler compounds MCoSb (M= Ti, Zr, Hf): a first principles study," *Materials Research Express*, vol. 6, no. 6, p. 066307, 2019.

[10] J. P. Perdew, K. Burke, and M. Ernzerhof, "Generalized gradient approximation made simple," *Physical review letters*, vol. 77, no. 18, p. 3865, 1996.

[11] G. Kresse and D. Joubert, "From ultrasoft pseudopotentials to the projector augmented-wave method," *Physical Review B*, vol. 59, no. 3, p. 1758, 1999.

[12] L. Schimka, J. Harl, and G. Kresse, "Improved hybrid functional for solids: The HSEsol functional," *The Journal of Chemical Physics*, vol. 134, no. 2, 2011.
[13] A. Togo and I. Tanaka, "First principles phonon calculations in materials science," *Scr. Mater.*, vol. 108, pp. 1–5, Nov 2015.
[14] A. Togo, "First-principles phonon calculations with phonopy and phono3py," *Journal of the Physical Society of Japan*, vol. 92, no. 1, p. 012001, 2023.
[15] A. Dwight, "Alloying behavior of zirconium, hafnium and the actinides in several series of isostructural compounds," *Journal of the Less Common Metals*, vol. 34, no. 2, pp. 279–284, 1974.
[16] A. Popoola and J. Lowther, "Computational study of platinum group superalloys," *International Journal of Modern Physics B*, vol. 28, no. 09, p. 1450066, 2014.
[17] W. G. Fahrenholtz, G. E. Hilmas, I. G. Talmy, and J. A. Zaykoski, "Refractory diborides of zirconium and hafnium," *Journal of the American Ceramic Society*, vol. 90, no. 5, pp. 1347–1364, 2007.
[18] J. P. Perdew and M. Levy, "Physical content of the exact kohn-sham orbital energies: band gaps and derivative discontinuities," *Physical Review Letters*, vol. 51, no. 20, p. 1884, 1983.
[19] F. Mouhat and F.-X. Coudert, "Necessary and sufficient elastic stability conditions in various crystal systems," *Physical Review B*, vol. 90, no. 22, p. 224104, 2014.
[20] A. Musari, B. Adetunji, P. Adebambo, and G. Adebayo, "Lattice dynamics and thermodynamic investigation of MNiSn (M= Hf, Ti and Zr) half-Heusler compounds: Density functional theory approach," *Materials Today Communications*, vol. 22, p. 100671, 2020.
[21] M. Ali and S. Naqib, "Recently synthesized $(Ti_{1-x}Mo_x)_2AlC$ solid solutions: deciphering the structural, electronic, mechanical and thermodynamic properties via ab initio simulations," *RSC advances*, vol. 10, no. 52, pp. 31 535–31 546, 2020.
[22] M. Rana, S. Islam, K. Hoque, G. Biswas, M. Hossain, S. Naqib, and M. A. Ali, "DFT prediction of the stability and physical properties of $M_2GaB$ (M= Sc, V, Nb, Ta)," *Journal of Materials Research and Technology*, vol. 24, pp. 7795–7815, 2023.
[23] M. Ali, M. Hossain, M. Uddin, M. Hossain, A. Islam, and S. Naqib, "Physical properties of new max phase borides $M_2SB$ (M= Zr, Hf and Nb) in comparison with conventional MAX phase carbides $M_2SC$ (M= Zr, Hf and Nb): Comprehensive insights," *Journal of Materials Research and Technology*, vol. 11, pp. 1000–1018, 2021.
[24] X.-Q. Chen, H. Niu, D. Li, and Y. Li, "Modeling hardness of polycrystalline materials and bulk metallic glasses," *Intermetallics*, vol. 19, no. 9, pp. 1275–1281, 2011.
[25] Y. Tian, B. Xu, and Z. Zhao, "Microscopic theory of hardness and design of novel superhard crystals," *International Journal of Refractory Metals and Hard Materials*, vol. 33, pp. 93–106, 2012.
[26] B. Mnisi, E. Benecha, and M. Tibane, "Density functional theory studies of structural, electronic and optical properties of cubic 3d-transition metal nitrides," *Intermetallics*, vol. 137, p. 107272, 2021.
[27] M. Fine, L. Brown, and H. Marcus, "Elastic constants versus melting temperature in metals," *Scripta metallurgica*, vol. 18, no. 9, pp. 951–956, 1984.
[28] M. W. Qureshi, M. Ali, and X. Ma, "Screen the thermomechanical and optical properties of the new ductile 314 MAX phase boride $Zr_3CdB_4$: A DFT insight," *Journal of Alloys and Compounds*, vol. 877, p. 160248, 2021.
[29] D. Alfè, "Phon: A program to calculate phonons using the small displacement method," *Computer Physics Communications*, vol. 180, no. 12, pp. 2622–2633, 2009.
[30] D. M. Rowe, *CRC handbook of thermoelectrics*. CRC press, 1995.
[31] S. N. Eliassen, A. Katre, G. K. Madsen, C. Persson, O. M. Løvvik, and K. Berland, "Lattice thermal conductivity of $Ti_xZr_yHf_{1-x-y}NiSn$ half-Heusler alloys calculated from first principles: Key role of nature of phonon modes," *Physical Review B*, vol. 95, no. 4, p. 045202, 2017.